**Science and Technology Indonesia**
*e*-ISSN:2580-4391 *p*-ISSN:2580-4405
Vol. 11, No. 2, April 2026

Research Paper

# Tuning Magnetic Behavior of $La_{1-x}Sr_xFeO_3$ (x = 0.1–0.5) via Sr Doping: From Antiferromagnetism to Ferromagnetism

Ramlan[1*], Marzuki Naibaho[2], Masno Ginting[3*]

[1]*Department of Physics, Faculty of Mathematic and Natural Sciences, Universitas Sriwijaya, Inderalaya, Ogan Ilir, South Sumatera, 30662, Indonesia*
[2]*Department of Physics, Universitas Indonesia, Depok, South Tangerang, 16424, Indonesia*
[3]*Research Center for Energy Materials (PRME) - National Research and Innovation Agency (BRIN), Complex Puspiptek Building 440-441, South Tangerang, 15314, Indonesia*
***Corresponding author**: ramlan@unsri.ac.id, masn001@brin.go.id

**Abstract**
Strontium-substituted $LaFeO_3$ compounds with the chemical formula $La_{1-x}Sr_xFeO_3$ (x = 0.1–0.5) were successfully prepared via the solid-state reaction technique by partially replacing La at the A-site. Structural analysis was performed using X-ray diffraction (XRD), while the surface morphology and elemental composition were investigated through scanning electron microscopy coupled with energy-dispersive X-ray spectroscopy (SEM–EDS). The magnetic behavior of the samples was evaluated using a vibrating sample magnetometer (VSM). XRD patterns verified that all synthesized compositions crystallized in a single-phase $LaFeO_3$ structure without detectable impurity phases. The dominant diffraction peak corresponded to the (121) crystallographic plane, confirming an orthorhombic structure with the Pnma space group (No. 62). SEM observations showed irregular particle shapes accompanied by a broad particle size distribution. EDS analysis confirmed the successful incorporation of Sr into the $LaFeO_3$ lattice, as evidenced by the presence of La, Fe, O, and Sr elements across all doped compositions (x = 0.1–0.5). Magnetic measurements revealed that the $La_{0.9}Sr_{0.1}FeO_3$ sample exhibited superior magnetic performance, with a saturation magnetization (Ms) of 0.393 T and a coercive field (Hc) of 2661 Oe. The introduction of Sr resulted in a transition of magnetic behavior from antiferromagnetic to ferromagnetic ordering. Overall, these results demonstrate that $La_{1-x}Sr_xFeO_3$ materials are promising candidates for electromagnetic wave absorption applications.

**Keywords**
$LaFeO_3$, Solid State Reaction, Structure, Morphology, Magnetic Properties

Received: 28 August 2025, Accepted: 4 February 2026
https://doi.org/10.26554/sti.2026.11.2.515-523

## 1. INTRODUCTION

Magnetic materials are essential components in various modern technological applications, ranging from permanent magnets, electronic devices, and energy systems to telecommunications (Edianta et al., 2021; Ramlan et al., 2024). Magnetic characteristics, including magnetic saturation (Ms), remanence (Mr), coercive field (Hc), and magnetic susceptibility (X), are highly dependent on the material's crystal lattice, microstructural features, and elemental composition (Melinia et al., 2024; Nasution et al., 2025; Novita et al., 2023, 2024). Through compositional engineering and synthesis methods, magnetic characteristics can be enhanced to produce materials with optimal performance tailored to specific applications. Among various magnetic materials, perovskite oxides ($ABO_3$) have emerged as attractive candidates due to their flexible crystal structure, excellent chemical stability, and tunable electrical and magnetic properties through ion substitution at the A or B sites (Pidburtnyi et al., 2021).

Perovskite oxides possess an $ABO_3$ crystal structure, where A is a cation with a large ionic radius and coordination number 12, while B is a cation with a coordination number of 6 (Pidburtnyi et al., 2021). Perovskite materials have attracted significant research interest due to their magnetic (Acharya et al., 2010, 2011), electrical (El-Mallah, 2012; Li and Zhu, 2021; Thirumalairajan et al., 2015), optical, and ferroelectric properties (Janbutrach et al., 2014). Their advantages lie in the wide compositional flexibility while retaining the fundamental perovskite structure, enabling their use in magnets, electronic devices, solar cells, and photocatalysts (Pidburtnyi et al., 2021). Perovskite materials have been widely studied in previous works, including $LaMnO_3$ (Zhang et al., 2013), $CaMnO_3$ (Su et al., 2023), $YFeO_3$ (Wang et al., 2021), $CoTiO_3$ (Yunasfi et al., 2025), $LaFeO_3$ (Huang et al., 2022), and many others. One particularly interesting perovskite oxide is $LaFeO_3$.

$LaFeO_3$ has attracted considerable research interest as an electrode material, catalyst, and sensor owing to its distinctive physical characteristics and broad application potential (Huang et al., 2020; Liu et al., 2017; Meng et al., 2024; Pidburtnyi et al., 2021). Extensive investigations have been conducted on its synthesis routes, structural features, and physicochemical properties. This material is classified as an antiferromagnetic insulator with a high Néel temperature ($T_n$ = 740 K) and is a member of the orthoferrite family. One of the most remarkable aspects of $LaFeO_3$ is the simultaneous presence of antiferromagnetic ordering and ferroelectric behavior at room temperature, which continues to draw significant attention from the physics and materials science communities. Structurally, $LaFeO_3$ crystallizes in an orthorhombic lattice with the Pbnm space group. The stability of perovskite structures is commonly assessed using the Goldschmidt tolerance factor (t), which is less than unity for $LaFeO_3$. This deviation induces a transformation from an ideal cubic structure to a distorted orthorhombic phase, characterized by Fe–O–Fe bond angles that differ from 180°, leading to distortions of the $FeO_6$ octahedra, as previously reported Huang et al. (2020, 2022). Owing to its chemical stability, environmental friendliness, and relatively narrow band gap, $LaFeO_3$ has been widely explored for advanced technological applications, including solar energy conversion devices (Ju et al., 2019), solid oxide fuel cell (SOFC) electrodes (Ju et al., 2019), gas sensing platforms (Hao et al., 2020), supercapacitor systems (Ata et al., 2025), photocatalytic processes (Ata et al., 2025), and microwave absorption materials (Yan et al., 2024).

In magnetism, perovskite oxide $LaFeO_3$ has been intensively investigated due to its remarkable physical properties such as superconductivity (Varignon, 2023), colossal magnetoresistance (Vitayaya et al., 2024), multiferroicity, magnetocaloric effect (Zhemas et al., 2025), thermoelectricity (Wu and Gao, 2018), spintronics (Bouhenna et al., 2025), absorbers (Naibaho et al., 2025; Sihotang et al., 2025), and many other applications for future technologies (Assirey, 2019). Alongside these advances, $LaFeO_3$ has been synthesized using various methods, including coprecipitation (Rianna et al., 2023), electrospinning (Jeong et al., 2018), sol-gel (Huang et al., 2022), hydrothermal (Mesbah et al., 2020), solid-state reaction, and wet mixing (Nehan et al., 2025; Zhang et al., 2013).

Naibaho et al. (2025) successfully synthesized single-phase $LaFeO_3$ as a microwave-absorbing material by varying the sintering temperature using the solid-state reaction method (Naibaho et al., 2025, 2024). In another study, Huang et al. (2022) synthesized $La_{1-x}Ba_xFeO_3$ (x=0.0-0.4) via the sol-gel method doped with $Ba^{2+}$, which enhanced its magnetic properties by inducing a transition from antiferromagnetic to ferromagnetic behavior and increasing microwave absorption (Huang et al., 2022). Similarly, in $YFeO_3$ synthesized via the sol-gel method doped with Sr, Man Wang reported that $Y_{1-x}Ba_xFeO_3$ samples transitioned from weak ferromagnetism to paramagnetism with increasing Sr content (Wang et al., 2021). Investigations on $La_{0.75}Sr_{0.25}MnO_3$ synthesized using the solid-state reaction method revealed an improvement in its magnetic properties (Zhang et al., 2013). Furthermore, $LaFeO_3$ synthesized via the sol-gel method with $Sr^{2+}$ doping demonstrated enhanced magnetic properties of $La_{1-x}Ba_xFeO_3$ samples as Sr content increased (Huang et al., 2020).

Based on previous studies, Sr doping has demonstrated great potential in enhancing the magnetic properties of $LaFeO_3$, particularly when synthesized using methods such as mechanical alloying and solution-based techniques like sol–gel. In this study, Sr-doped $LaFeO_3$ will be synthesized via the solid-state reaction method using an agate mortar. This approach is employed as a comparative synthesis route due to its simplicity, environmental friendliness, and suitability for large-scale production without generating acidic or basic waste. The main focus of this research is to investigate the effect of Sr doping on the crystal structure, morphology, and magnetic properties of $LaFeO_3$, specifically saturation magnetization (Ms), coercivity (Hc), and remanence (Mr).

## 2. EXPERIMENTAL SECTION

### 2.1 Materials

The precursors were provided by LOBA CHEMIE PVT. LTD., Indonesia, and included 99.5% pure lanthanum oxide ($La_2O_3$), >99% pure iron (III) oxide ($Fe_2O_3$), and >99% pure strontium carbonate ($SrCO_3$).

### 2.2 Methods

A compound of $LaFeO_3$ by mixing solid powders. We started with $La_2O_3$, $SrCO_3$, and $Fe_2O_3$ powders, measured them out based on the right amounts, and then mashed them together in a mortar for an hour. After that, we put the mix in an oven to dry at 90°C for half a day. Then, we heated it up really hot, to 1200°C, for 5 hours. Once it was all baked, we ground it up again with a mortar and sifted it through a fine 200-mesh sieve. Finally, we checked out the powders we got using a bunch of different tools: X-ray Diffraction (XRD, SmartLab Rigaku), Scanning Electron Microscopy (SEM), Energy Dispersive Spectroscopy (EDS, Phenom Pharos Desktop FEG), Fourier Transform Infrared Spectroscopy (FTIR, Bruker Alpha II), and Vibrating Sample Magnetometry (VSM, Oxford 1.2H).

## 3. RESULTS AND DISCUSSION

### 3.1 XRD Analysis of $La_{1-x}Sr_xFeO_3$

The X-ray diffraction (XRD) patterns of $La_{1-x}Sr_xFeO_3$ samples (x = 0, 0.1, 0.3, 0.5) were analyzed using Cu-K$\alpha$ radiation ($\lambda$ = 0.15406 nm) at room temperature, within the 2$\theta$ range of 10–90°, as shown in Figure 1.

As seen in Figure 1, all samples' X-ray diffraction peaks suggest that the $LaFeO_3$ phase formed without the presence of secondary phases. The (121) plane, which corresponds to the $LaFeO_3$ phase, can be identified as the primary peak found. As Sr doping increased, the diffraction peaks gradually shifted toward higher angles and their intensity decreased, as seen in Figure 1b. As shown in Figure 2 and verified by COD

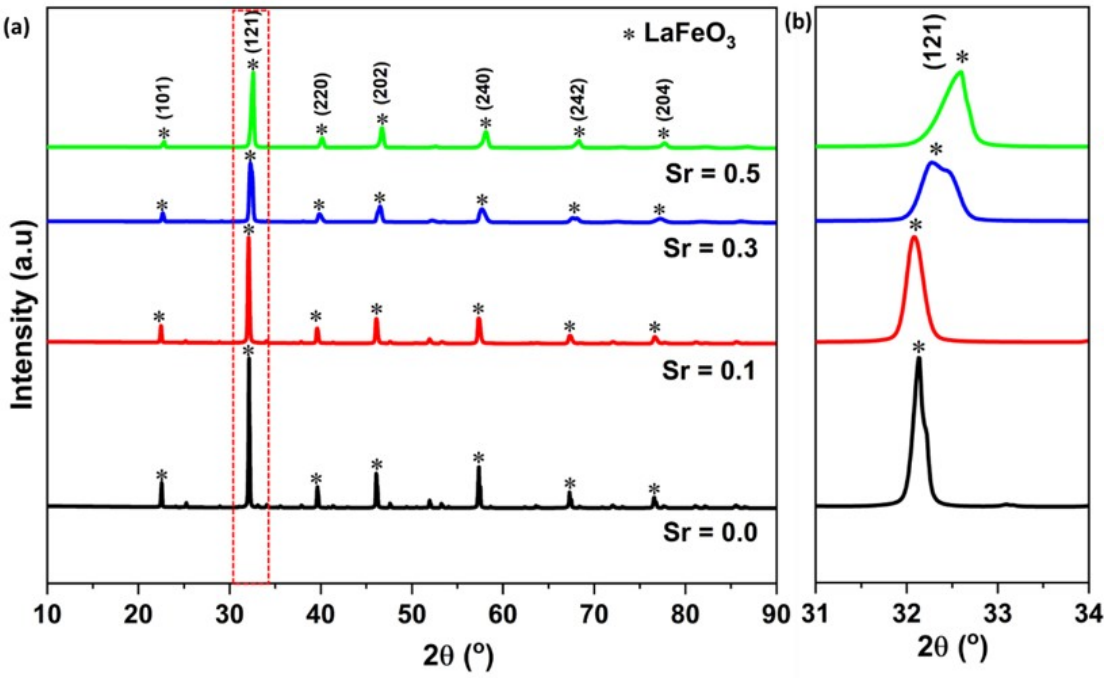


**Figure 1.** (a) XRD Patterns of $La_{1-x}Sr_xFeO_3$ (x = 0, 0.1, 0.3, 0.5), (b) hkl (121) Peak

**Table 1.** XRD Parameters of $La_{1-x}Sr_xFeO_3$

| Sample | Structure | FWHM | 2θ | Lattice parameter (Å) | | | Crystallite size (Å) | Volume (Å) |
|---|---|---|---|---|---|---|---|---|
| | | | | a | b | c | | |
| Sr = 0.0 | Orthorhombic | 0.099 | 32.115 | 5.563 | 7.851 | 5.552 | 80.694 | 242.479 |
| Sr = 0.1 | Orthorhombic | 0.154 | 32.154 | 5.549 | 7.850 | 5.533 | 51.565 | 241.057 |
| Sr = 0.3 | Orthorhombic | 0.312 | 32.345 | 5.533 | 7.843 | 5.495 | 25.476 | 238.449 |
| Sr = 0.5 | Orthorhombic | 0.330 | 32.484 | 5.525 | 7.831 | 5.492 | 21.500 | 237.618 |

**Table 2.** EDX Result of $La_{1-x}Sr_xFeO_3$ ($x$ = 0, 0.1, 0.3, 0.5)

| Element Symbol | Element Name | Sr = 0.0 | | Sr = 0.1 | | Sr = 0.3 | | Sr = 0.5 | |
|---|---|---|---|---|---|---|---|---|---|
| | | At (%) | Wt (%) | At (%) | Wt (%) | At (%) | Wt (%) | At (%) | Wt (%) |
| $La_{(57)}$ | Lanthanum | 57.33 | 65.36 | 23.87 | 61.42 | 12.62 | 39.07 | 10.20 | 32.51 |
| $Sr_{(38)}$ | Strontium | – | – | 2.41 | 3.91 | 10.36 | 20.24 | 12.49 | 25.10 |
| $Fe_{(26)}$ | Iron | 25.49 | 16.93 | 17.35 | 17.96 | 14.90 | 18.54 | 15.33 | 19.64 |
| $O_{(8)}$ | Oxygen | 17.18 | 17.71 | 56.37 | 16.71 | 62.12 | 22.15 | 61.98 | 22.75 |

PDF#1526450, the diffraction peak seen in the (121) plane may be indexed to the conventional $LaFeO_3$ phase with an orthorhombic structure (Pnma, space group 62). These findings imply that the solid-state reaction mechanism can be used to insert $Sr^{2+}$ ions into the $LaFeO_3$ perovskite lattice. Furthermore, the XRD parameters provide a clearer explanation of the relationship between Figure 1 and Table 1.

The revised crystal structure and lattice properties of $LaFeO_3$ derived from the Rietveld refinement study are shown in Table 1. Equation (1) provides the full width at half maximum (FWHM) of the (121) peak based on the Debye–Scherrer technique, which was used to compute the crystallite size. The results are reported in Table 1.

$$D = \frac{K\lambda}{\beta \cos\theta} \quad (1)$$

where $K$, $\lambda$, and $\beta$ stand for the Scherrer constant, the X-ray wavelength, and the observed FWHM of the diffraction peak, respectively, and $D$ is the average crystallite size perpendicular to the crystal plane.

Table 1 illustrates how the crystallite size of $La_{1-x}Sr_xFeO_3$ reduces as Sr doping increases. The substitution of $La^{3+}$ (0.106 nm), which has a smaller ionic radius, for $Sr^{2+}$ (0.113 nm),

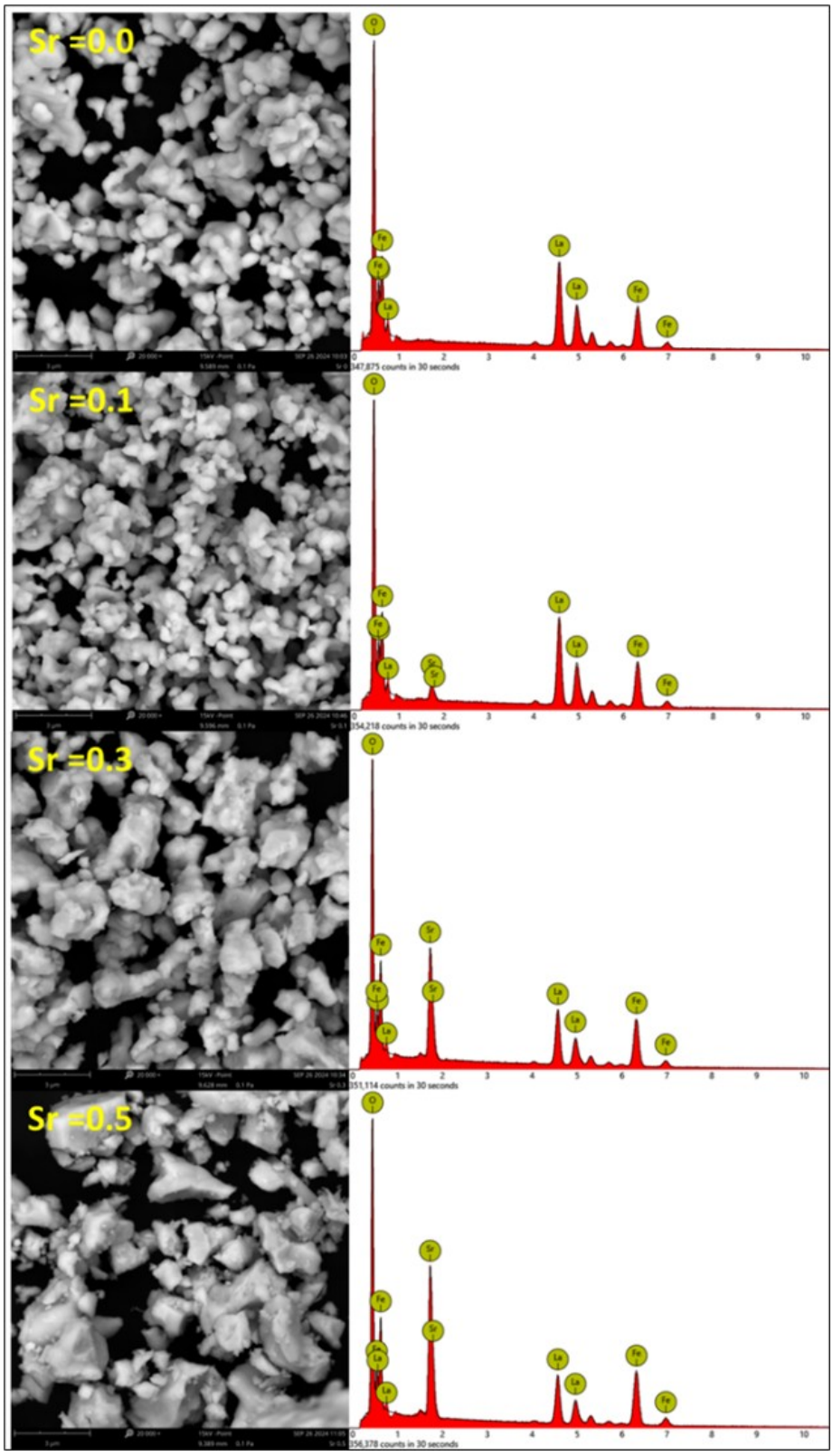


**Figure 2.** SEM-EDS Micrographs of $La_{1-x}Sr_xFeO_3$ (x = 0, 0.1, 0.3, 0.5)

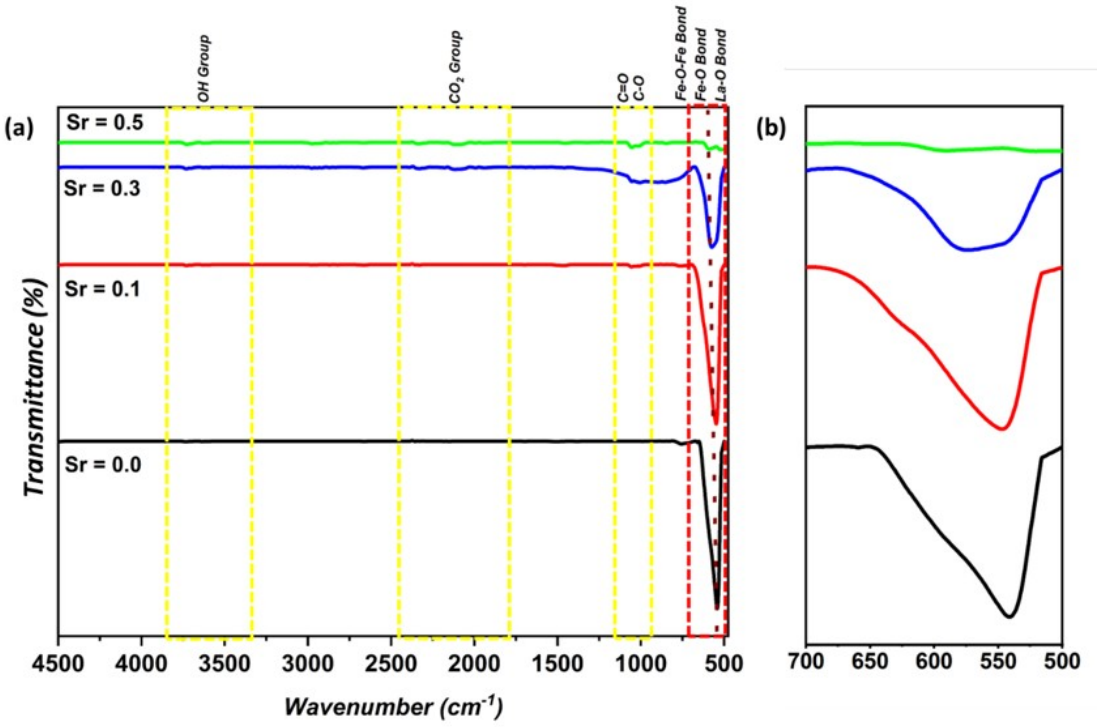


**Figure 3.** FTIR Spectra of $La_{1-x}Sr_xFeO_3$ (x = 0, 0.1, 0.3, 0.5) with the Wavenumber Range (a) 4500-500 $cm^{-1}$, and (b) 700-500 $cm^{-1}$

**Table 3.** Result of the Magnetic Properties of $La_{1-x}Sr_xFeO_3$ ($x$ = 0.0, 0.1, 0.3, 0.5)

| Sample | Ms (emu/g) | Mr (emu/g) | Hc (T) | Squareness (Mr/Ms) |
|---|---|---|---|---|
| Sr = 0.0 | 0.094 | 0.017 | 0.036 | 0.181 |
| Sr = 0.1 | 2.66 | 1.66 | 0.393 | 0.062 |
| Sr = 0.3 | 2.16 | 1.39 | 0.23 | 0.643 |
| Sr = 0.5 | 1.62 | 0.70 | 0.12 | 0.432 |

which has a greater ionic radius, may be connected to this occurrence. Under the same sintering temperature and time, materials with larger ionic radii for all samples require more crystallization energy than those with smaller ionic radii. As the concentration of $Sr^{2+}$ rises, the crystallite size decreases because $La_{1-x}Sr_xFeO_3$ nanoparticles have insufficient crystallization energy (Huang et al., 2020). Furthermore, when the Sr content increases, the unit cell volume of $LaFeO_3$ declines and reaches a minimum at x = 0.5 Sr doping. It is clear that the unit cell volume and crystallite size.

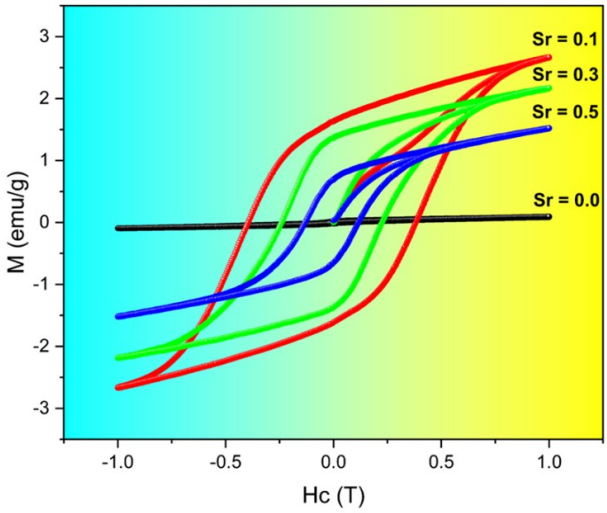


**Figure 4.** Hysteresis Loops of $La_{1-x}Sr_xFeO_3$ (x= 0.0, 0.1, 0.3, 0.5)

### 3.2 SEM-EDS Analysis Of $La_{1-x}Sr_xFeO_3$

The SEM-EDS results of samples sintered for five hours at 1200°C are shown in Figure 2. The pictures demonstrate that when Sr doping increases, particle aggregation becomes more noticeable and interparticle spacing reduces. When examined at a 20,000× magnification, the particle size falls between 1 and 3 $\mu$m. Table 2 summarizes the relevant EDX results,

**Table 4.** Comparison of Lanthanum Ferrite-Based Magnetic Properties Research

| Materials | Method | Ms (emu/g) | Mr (emu/g) | Hc (Oe) | References |
|---|---|---|---|---|---|
| $LaFe_{0.50}Co_{0.50}O_3$ | Sol–Gel | – | 0.07 | 408 | (La et al., 2022a) |
| $La_{0.9}Bi_{0.1}Fe_{0.50}Co_{0.50}O_3$ | | | 0.01 | 593 | (La et al., 2022a) |
| $La_{0.8}Bi_{0.2}Fe_{0.50}Co_{0.50}O_3$ | | – | 0.085 | 3572 | (La et al., 2022a) |
| $BaSnO_3$ | Citric Acid-Assisted Combustion | 0.0023 | 0.0007 | 330 | (Handal et al., 2020) |
| $BaSn_{0.99}Gd_{0.01}O_3$ | | 0.005 | 0.0011 | 240 | (Handal et al., 2020) |
| $BaSn_{0.98}Gd_{0.01}Mn_{0.01}O_3$ | | 0.024 | 0.017 | 2578 | (Handal et al., 2020) |
| $BaSn_{0.95}Gd_{0.01}Mn_{0.04}O_3$ | | 0.106 | 0.055 | 1578 | (Handal et al., 2020) |
| $BaSn_{0.98}Gd_{0.01}Ni_{0.01}O_3$ | | 0.049 | 0.031 | 1117 | (Handal et al., 2020) |
| $BaSn_{0.95}Gd_{0.01}Ni_{0.04}O_3$ | | 0.0135 | 0.004 | 386 | (Handal et al., 2020) |
| $Ba_{0.3}La_{0.7}Ti_{0.3}Fe_{0.7}O_3$ | Solid State Reaction | 1.23 | 0.52 | 179.52 | (La et al., 2022b) |
| $Ba_{0.1}La_{0.9}Ti_{0.1}Fe_{0.9}O_3$ | | 7.61 | 3.60 | 20.38 | (La et al., 2022b) |
| $YFeO_3$ | Sol–Gel | 0.3319 | 0.1362 | 10472.06 | (Wang et al., 2021) |
| $Y_{0.95}Sr_{0.05}FeO_3$ | | 0.3853 | 0.1495 | 9602.55 | (Wang et al., 2021) |
| $Y_{0.90}Sr_{0.10}FeO_3$ | | 0.4290 | 0.1586 | 7524.34 | (Wang et al., 2021) |
| $Y_{0.85}Sr_{0.15}FeO_3$ | | 0.9797 | 0.3218 | 1463.35 | (Wang et al., 2021) |
| $La_{0.75}Gd_{0.25}FeO_3$ | Solid-State Reaction | 0.72 | 0.169 | 2700 | (Saikia et al., 2022) |
| $LaFeO_3$ | Citrate–Nitrate Auto Combustion | 0.300 | 0.049 | 257.08 | (Ateia et al., 2021) |
| $Ce_{0.7}La_{0.3}FeO_3$ | | 1.351 | 0.168 | 192.38 | (Ateia et al., 2021) |
| $Pr_{0.7}La_{0.3}FeO_3$ | | 0.353 | 0.024 | 220.64 | (Ateia et al., 2021) |
| $Nd_{0.7}La_{0.3}FeO_3$ | | 0.284 | 0.011 | 387.39 | (Ateia et al., 2021) |
| $Sm_{0.7}La_{0.3}FeO_3$ | | 0.447 | 0.191 | 4848.8 | (Ateia et al., 2021) |
| $Gd_{0.7}La_{0.3}FeO_3$ | | 1.771 | 0.027 | 158.71 | (Ateia et al., 2021) |
| $La_{0.6}Ba_{0.4}FeO_3$ | Sol–Gel | – | 0.0125 | 750 | (Huang et al., 2022) |
| $LaFeO_3$ | Hydrothermal | 0.0036 | 0.00037 | 1044.79 | (Sasikala et al., 2019) |
| $LaFe_{0.8}Ti_{0.2}O_3$ | | 0.0074 | 0.00035 | 448.31 | (Sasikala et al., 2019) |
| $LaFe_{0.6}Ti_{0.4}O_3$ | | 0.0099 | 0.00061 | 339.39 | (Sasikala et al., 2019) |
| $LaFe_{0.4}Ti_{0.6}O_3$ | | 0.0028 | 0.00016 | 623.61 | (Sasikala et al., 2019) |
| $LaFeO_3$ | Sol–Gel | 0.1256 | 0.0032 | 22.6 | (Huang et al., 2020) |
| $La_{0.9}Sr_{0.1}FeO_3$ | | 0.1581 | 0.0093 | 566.72 | (Huang et al., 2020) |
| $La_{0.8}Sr_{0.2}FeO_3$ | | 0.2906 | 0.0611 | 2978.79 | (Huang et al., 2020) |
| $La_{0.7}Sr_{0.3}FeO_3$ | | 0.3903 | 0.1442 | 3551.50 | (Huang et al., 2020) |
| $La_{0.6}Sr_{0.4}FeO_3$ | | 0.8102 | 0.3129 | 4145.53 | (Huang et al., 2020) |
| $LaFeO_3$ | Solid State Reaction | 0.094 | 0.017 | 360 | This Work |
| $La_{0.9}Sr_{0.1}FeO_3$ | | 2.661 | 1.66 | 3930 | This Work |
| $La_{0.7}Sr_{0.3}FeO_3$ | | 2.160 | 1.39 | 2300 | This Work |
| $La_{0.5}Sr_{0.5}FeO_3$ | | 1.620 | 0.70 | 1200 | This Work |

which demonstrate that as Sr doping increases, the intensity and weight % of La drop.

In this instance, the FTIR spectra of the $La_{1-x}Sr_xFeO_3$ samples are influenced by the structure, crystallite size, unit cell volume, and EDX results.

### 3.3 FTIR Analysis of $La_{1-x}Sr_xFeO_3$

The FTIR spectra of $La_{1-x}Sr_xFeO_3$ (x = 0.0–0.5) reveal the characteristic vibrational features of the perovskite lattice and clearly demonstrate the influence of Sr substitution on the local bonding environment. A broad absorption band observed in the range of 3400–3600 $cm^{-1}$ is attributed to the stretching vibration of –OH groups, originating from adsorbed moisture or surface-bound water molecules. The weak bands appearing around 2000–2400 $cm^{-1}$ are associated with adsorbed $CO_2$ species from the ambient atmosphere, while the absorption features in the 980–1200 $cm^{-1}$ region correspond to C=O and C–O vibrational modes, which are commonly linked to residual carbonate species formed during the solid-state synthesis process. The most prominent and structurally significant absorption occurs in the low-wavenumber region, particularly between 500 and 600 $cm^{-1}$, which is assigned to the stretching vibrations of Fe–O and La–O bonds within the $FeO_6$ octahedra, confirming the formation of the $La_1FeO_3$ perovskite

framework. Notably, variations in the intensity and slight shifts of the Fe−O¯related bands with increasing Sr content indicate lattice distortion and modifications in bond lengths and bond angles induced by the substitution of $Sr^{2+}$ for $La^{3+}$ at the A-site. Such local structural distortions are known to play a crucial role in tailoring the magnetic and electromagnetic responses of perovskite oxides, thereby enhancing their suitability for electromagnetic wave absorption applications. These observations are consistent with previous studies reporting that alkaline-earth doping in $LaFeO_3$ significantly alters lattice vibrations and local structural characteristics (Huang et al., 2020; Nehan et al., 2025; Pidburtnyi et al., 2021). In this instance, the Magnetic properties of the $La_{1-x}Sr_xFeO_3$ samples are influenced by the FTIR spectra.

### 3.4 Magnetic Properties of $La_{1-x}Sr_xFeO_3$

The magnetic hysteresis loops of the samples produced at room temperature under an applied magnetic field of 1.2 T are shown in Figure 4, illustrating the measurement of the magnetic properties of $LaFeO_3$ crystals using VSM.

First, with saturation magnetization (Ms), remanence (Mr), and coercivity (Hc) values of 0.094 emu/g, 0.017 emu/g, and 0.036 T, respectively, the $LaFeO_3$ particles without Sr doping show a comparatively low hysteresis curve (Table 3). This suggests that the presence of $Fe^{3+}$ ion interactions and antiparallel interactions causes pure $LaFeO_3$ to be a weak ferromagnet. At ambient temperature, pure $LaFeO_3$ is also known to exhibit G-type antiferromagnetic activity. Both Ms and Hc values rise with Sr doping, as Table 4 illustrates, reaching maximum values of 2.661 emu/g, 1.66 emu/g, and 0.393 T, respectively, for $La_{0.9}Sr_{0.1}FeO_3$. This implies that the material experiences a change in behavior from antiferromagnetic (AFM) to ferromagnetic (FM) (Wang et al., 2021). Lattice expansion and structural distortion brought on by the substitution of (0.113 nm), which has a greater ionic radius, for $La^{3+}$ (0.106 nm), which has a smaller ionic radius, can account for the increase in magnetism. The resulting structural changes lead to a reduction in the Fe–O–Fe bond angle, as reported in previous studies (Huang et al., 2020). AFM superexchange interactions strengthen with increasing Fe–O–Fe bond angle, with the maximum at 180° (Huang et al., 2020; Zhang et al., 2013). Therefore, the reduction of this bond angle weakens AFM superexchange interactions, thereby deviating the structure from its AFM nature. Furthermore, this also promotes the formation of oxygen vacancies and multivalent iron ions, which typically occur during high-temperature sintering of $LaFeO_3$ under an oxygen atmosphere. The substitution of $Sr^{2+}$ for $La^{3+}$ enhances the Fe ion states, leading to improved magnetic properties.

## 4. CONCLUSIONS

The perovskite material $LaFeO_3$ is an oxide with an orthorhombic structure that exhibits intriguing magnetic and functional properties. In this study, Sr doping on $LaFeO_3$ was carried out using the solid-state reaction method, which revealed changes in structure, morphology, and magnetic properties. XRD analysis showed that all samples retained the $LaFeO_3$ structure without secondary phases; however, diffraction peak shifts and a gradual decrease in intensity were observed with increasing Sr doping. The incorporation of Sr led to a reduction in crystallite size from 80.694 to 21.500 Åand a decrease in unit cell volume from 242.479 Å. SEM analysis indicated that particle sizes were in the range of 1–3 $\mu$m, and no other elements were detected besides La, Fe, O, and the doped Sr, as confirmed by EDS. Regarding magnetic properties, Sr doping enhanced the saturation magnetization (2.66 emu/g), remanence (1.66 emu/g), and coercivity (0.393 T), with the maximum values observed in $La_{0.9}Sr_{0.1}FeO_3$. This enhancement is attributed to lattice distortion and modifications in Fe–O–Fe interactions, which promote a transition from antiferromagnetic to ferromagnetic behavior. Therefore, Sr doping is proven to improve the magnetic performance of $LaFeO_3$, making it promising for various technological applications such as sensors, electrodes, and microwave absorbers.

## 5. ACKNOWLEDGMENT

The authors would like to express their sincere gratitude to the Characterization Laboratory, National Research and Innovation Agency (BRIN), for providing access to the characterization facilities (XRD, SEM-EDS, and VSM) used in this study.

## REFERENCES

Acharya, S., A. K. Deb, D. Das, and P. K. Chakrabarti (2011). Enhanced Magnetic Behavior of Al-Substituted LaFeO3 ($La_{1-x}Al_xFeO_3$, $x$ = 0.10 and 0.30). *Materials Letters*, **65**(9); 1280–1282

Acharya, S., J. Mondal, S. Ghosh, S. K. Roy, and P. K. Chakrabarti (2010). Multiferroic Behavior of Lanthanum Orthoferrite ($LaFeO_3$). *Materials Letters*, **64**(3); 415–418

Assirey, E. A. R. (2019). Perovskite Synthesis, Properties and Their Related Biochemical and Industrial Applications. *Saudi Pharmaceutical Journal*, **27**(6); 817–829

Ata, S., I. Shaheen, A. Bibi, H. Elhouichet, A. Nazir, M. Iqbal, and J. Shawaf (2025). Supercapacitor and Photocatalytic Potential of Aluminium and Zinc-Doped $LaFeO_3$ Perovskite Synthesized by Hydrothermal Route. *Journal of the Korean Ceramic Society*; 1–12

Ateia, E. E., H. Ismail, H. Elshimy, and M. K. Abdelmaksoud (2021). Structural and Magnetic Tuning of $LaFeO_3$ Orthoferrite Substituted with Different Rare Earth Elements to Optimize Their Technological Applications. *Journal of Inorganic and Organometallic Polymers and Materials*, **31**(4); 1713–1725

Bouhenna, A., A. Azzouz-Rached, W. Mohammed, O. Zeggai, N. Sfina, N. Rahman, M. Husain, M. Fellah, Y. Alawaideh, and M. Uzair (2025). First-Principles Calculations to Investigate Physical Properties of Oxide Perovskites LaBO3 (B = Mn, Fe) for Thermo-Spintronic Devices. *Journal of Physics and Chemistry of Solids*, **196**; 112362

 

Edianta, J., N. Fauzi, M. Naibaho, F. S. Arsyad, and I. Royani (2021). Review of the Effectiveness of Plant Media Extracts in Barium Hexaferrite Magnets ($BaFe_{12}O_{19}$). *Science and Technology Indonesia*, **6**(2); 39–52

El-Mallah, H. M. (2012). AC Electrical Conductivity and Dielectric Properties of Perovskite (Pb, Ca) $TiO_3$ Ceramic. *Acta Physica Polonica A*, **122**(1); 174–179

Handal, H. T., H. A. Mousa, S. M. Yakout, W. Sharmoukh, and V. Thangadurai (2020). Effect of Mn and Ni Doping on Structure, Photoluminescence, and Magnetic Properties. *Journal of Magnetism and Magnetic Materials*, **498**; 165946

Hao, P., G. Qiu, P. Song, Z. Yang, and Q. Wang (2020). Construction of Porous $LaFeO_3$ Microspheres Decorated with NiO Nanosheets for High-Response Ethanol Gas Sensors. *Applied Surface Science*, **515**; 146025

Huang, L., L. Cheng, S. Pan, Y. He, C. Tian, J. Yu, and H. Zhou (2020). Effects of Sr Doping on the Structure, Magnetic Properties, and Microwave Absorption Properties of $LaFeO_3$ Nanoparticles. *Ceramics International*, **46**(17); 27352–27361

Huang, L., L. Cheng, S. Pan, Q. Yao, Q. Long, M. Wang, Y. Chen, and H. Zhou (2022). Influence of A-Site Barium Doping on Structure, Magnetic, and Microwave Absorption Properties of $LaFeO_3$ Ceramic Powders. *Journal of Rare Earths*, **40**(7); 1106–1117

Janbutrach, Y., S. Hunpratub, and E. Swatsitang (2014). Ferromagnetism and Optical Properties of $La_{1-x}Al_xFeO_3$ Nanopowders. *Materials Research*; 1–7

Jeong, J. H., C. G. Song, K. H. Kim, W. Sigmund, and J. W. Yoon (2018). Effect of Mn Doping on Particulate Size and Magnetic Properties of $LaFeO_3$ Nanofibers Synthesized by Electrospinning. *Journal of Alloys and Compounds*, **749**; 599–604

Ju, Y., S. Lee, B. Su, and H. Ho (2019). Phase Transition of Doped $LaFeO_3$ Anode in Reducing Atmosphere and Their Power Generation Property in Intermediate Temperature Solid Oxide Fuel Cell. *International Journal of Hydrogen Energy*, **44**(56); 29641–29647

La, B., T. Fe, F. El, Z. Chchiyai, Y. Tamraoui, H. El, J. Alami, and B. Manoun (2022a). Effects of Bi Doping on Structural and Magnetic Properties of Cobalt Ferrite. *Ceramics International*, **48**(11); 16348–16356

La, B., T. Fe, F. El, Z. Chchiyai, Y. Tamraoui, H. El, J. Alami, and B. Manoun (2022b). Optical and Magnetic Properties of Perovskite Materials. *Journal of Rare Earths*, **40**(4); 652–659

Li, Q. and G. Zhu (2021). Controlling Negative Permittivity and Permeability Behavior in $LaFeO_3$ through Sintering Temperature. *Ceramics International*, **47**(4); 5244–5248

Liu, X., L. S. Wang, Y. Ma, H. Zheng, L. Lin, Q. Zhang, Y. Chen, Y. Qiu, and D. L. Peng (2017). Enhanced Microwave Absorption Properties by Tuning Cation Deficiency of Perovskite Oxides of Two-Dimensional $LaFeO_3$/C Composite in X-Band. *ACS Applied Materials & Interfaces*, **9**(8); 7601–7610

Melinia, L. A., M. Naibaho, E. Puspita, Ramlan, and M. Ginting (2024). Review on the Adsorption of Heavy Metals in Water by $MnFe_2O_4$ and Zeolite. *Indonesian Physical Review*, **6**(2); 196–219

Meng, F., L. Qin, H. Gao, H. Zhu, and Z. Yuan (2024). Perovskite-Structured $LaFeO_3$ Modified $In_2O_3$ Gas Sensor with High Selectivity and Ultra-Low Detection Limit for 2-Butanone. *Journal of Alloys and Compounds*, **970**; 172464

Mesbah, M., S. Hamedshahraki, S. Ahmadi, M. Sharifi, and C. A. Igwegbe (2020). Hydrothermal Synthesis of $LaFeO_3$ Nanoparticles Adsorbent: Characterization and Application of Error Functions for Adsorption of Fluoride. *MethodsX*, **7**; 100786

Naibaho, M., A. Mulyawan, P. Zhemas, Z. Nehan, W. A. Adi, B. Kurniawan, W. Hung, J. Widakdo, and M. Ginting (2025). Temperature-Dependent Phase Evolution and Reflection Loss of Lanthanum Orthoferrite ($LaFeO_3$). *Inorganic Chemistry Communications*, **176**; 114246

Naibaho, M., J. Widakdo, B. Kurniawan, P. Z. Z. Nehan, O. Vitayaya, Novita, Ramlan, and W. A. Adi (2024). Analysis of Structure, Morphology, Magnetic Properties, and Microwave Absorption of Lanthanum Orthoferrite ($LaFeO_3$). *Science and Technology Indonesia*, **9**(4); 1–6

Nasution, N., S. Humaidi, E. Frida, T. N. Duma, P. Zhemas, Z. Nehan, M. Naibaho, and M. Ginting (2025). The Influence of Yttrium Doping on the Microstructure and Magnetic Properties of Barium Hexaferrite. *Journal of Physics*, **22**(12); 13–15

Nehan, P. Z. Z., O. Vitayaya, D. R. Munazat, M. Naibaho, and M. T. E. Manawan (2025). Compound Synthesized by Solid-State, Sol-Gel, and Wet-Mixing Methods. *Materials Science Forum*, **1152**; 45–54

Novita, N., M. Naibaho, E. Puspita, Ramlan, M. Ginting, and S. Humaidi (2023). Analysis of Mineral Content and Magnetic Properties of Iron Sand of Bah Bolon Simalungun River, North Sumatera. *Asian Journal of Engineering, Social and Health*, **2**(12); 1633–1639

Novita, N., Ramlan, M. Naibaho, M. Ginting, S. Humaidi, and T. N. Duma (2024). $LaFeO_3$ Review: Nanostructure, Synthesis Methods, and Applications. *International Journal of Social Service and Research*, **4**(2); 539–559

Pidburtnyi, M., B. Zanca, C. Coppex, S. Jimenez-Villegas, and V. Thangadurai (2021). A Review on Perovskite-Type $LaFeO_3$-Based Electrodes for $CO_2$ Reduction in Solid Oxide Electrolysis Cells. *Chemistry of Materials*, **33**(12); 4249–4268

Ramlan, B. Soerya, A. Fachredzy, M. Naibaho, and M. Ginting (2024). Effect of Silicon Rubber (SIR) in Fabrication of NdFeB/$BaFe_{12}O_{19}$-Based Hybrid Magnet. *Indonesian Physical Review*, **7**(1); 114–123

Rianna, M., T. Sembiring, E. Amiruddin, and P. Sebayang (2023). Co-Precipitation Synthesis of LaFe1-xAlxO3 (x = 0–0.2) on Structure and Electromagnetic Properties. *Materials Science for Energy Technologies*, **6**; 43–47

Saikia, N., R. Chakravarty, S. Bhattacharjee, R. L. Hota, R. K. Parida, and B. N. Parida (2022). Synthesis and Characteriza-

 

tion of Gd-Doped $LaFeO_3$ for Device Application. *Materials Science in Semiconductor Processing*, **151**; 106969

Sasikala, C., G. Suresh, N. Durairaj, I. Baskaran, B. Sathyaseelan, E. Manikandan, R. Srinivasan, and M. K. Moodley (2019). Chemical, Morphological, Structural, Optical, and Magnetic Properties of Transition Metal Titanium (Ti)-Doped $LaFeO_3$ Nanoparticles. *Journal of Superconductivity and Novel Magnetism*, **32**(6); 1791–1797

Sihotang, M. S., M. A. Angelo, M. Naibaho, N. Ichsan, and M. Ginting (2025). Effect of Barium Hexaferrite Doped Yttrium (Y3+) on the Microwave Absorption by Solid-State Reaction Methods. *Journal of Technology and Physics*, **7**(1); 63–70

Su, J., H. Zhao, R. Yang, B. Wang, Y. Xu, X. Lin, Y. Xie, and C. Wang (2023). Thin La-Doped $CaMnO_3$ Ceramics for Attenuation–Impedance Balance to Facilitate Excellent Microwave Absorption. *Ceramics International*, **49**(19); 32049–32057

Thirumalairajan, S., K. Girija, V. R. Mastelaro, and N. Ponpandian (2015). Investigation on Magnetic and Electric Properties of Morphologically Different Perovskite $LaFeO_3$ Nanostructures. *Journal of Materials Science: Materials in Electronics*, **26**(11); 8652–8662

Varignon, J. (2023). Origin of Superconductivity in Hole-Doped $SrBiO_3$ Bismuth Oxide Perovskite from Parameter-Free First-Principles Simulations. *npj Computational Materials*, **9**; 1–8

Vitayaya, O., Z. Zul, and R. Munazat (2024). Magnetoresistance (MR) Properties of Magnetic Materials. *RSC Advances*, **14**; 18617–18645

Wang, M., L. Cheng, L. Huang, S. Pan, Q. Yao, C. Hu, Q. Liang, and H. Zhou (2021). Effect of Sr-Doped $YFeO_3$ Rare Earth Orthoferrite on Structure, Magnetic Properties, and Microwave Absorption Performance. *Ceramics International*, **47**(24); 34159–34169

Wu, T. and P. Gao (2018). Development of Perovskite-Type Materials for Applications. *Materials*, **11**(6); 999

Yan, L., Y. Zhang, Y. Zhang, R. Liu, C. Liu, F. Wu, X. Miao, E. Liu, X. Peng, J. Li, S. Tao, and F. Xu (2024). Influence of Bi Doping on the Structure and Electromagnetic Wave Absorption for $LaFeO_3$ Perovskite. *Journal of Magnetism and Magnetic Materials*, **591**; 171730

Yunasfi, Y., J. Setiawan, M. Mashadi, D. S. Winatapura, and M. Puspitasari (2025). Cationic Distribution Analysis of Lanthanum-Doped Cobalt Nickel Titanate as Microwave Absorbing Material and Its Correlation with Weak Ferromagnetic Behavior. *Journal of Magnetism*; 1–18

Zhang, S., Q. Cao, M. Zhang, and X. Shi (2013). Effects of $Sr^{2+}$ or $Sm^{3+}$ Doping on Electromagnetic and Microwave Absorption Performance of $LaMnO_3$. *Journal of Applied Physics*, **113**(7); 073905

Zhemas, P., Z. Nehan, B. Kurniawan, D. Rezky, O. Vitayaya, M. Naibaho, T. Sudiro, M. T. E. Manawan, Darminto, and H. Nojiri (2025). Calcium Ion Deficiency and Its Influence on Structure and Critical Behavior. *Journal of Alloys and Compounds*, **1020**; 179467

 